

Effect of Orientation and Temperature on Edge Crack Propagation of Bcc Iron under Cyclic Loading

L Ma*, C S Li and J R Guo

College of Physics and Electronic Science, Hunan University of Arts and Science, Changde 41500 China

Corresponding author and e-mail: L Ma, mlml6277@126.com

Abstract. The fatigue crack propagation behaviour with pre-existing edge crack was investigated in iron single crystal by molecular dynamics simulation. The results showed that the deformation characteristics of crack tip were influenced by the orientation of initial crack. The (010) [001] crack presented ductile fracture and the slip bands of crack tip were $\{110\}\langle 111\rangle$ systems at room temperature. Nevertheless, the $(\bar{1}10)$ [110] crack presented brittle rupture and the slip bands of crack tip were (011) $[1\bar{1}1]$ system. In (111) $[11\bar{2}]$ crack, the main deformation of crack tip was vacancies and dislocations at room temperature. The influence of temperature on the propagation of crack was also discussed in all crack models, the results revealed that the crack growth rate and the deformation mechanisms of crack tip changed as the temperature rose, and the threshold values of stress intensity factor decreased with the increasing temperature.

1. Introduction

The behaviour of fatigue crack propagation has a significant influence on the fracture properties of metallic materials. The studies of experimental and theoretical indicate that the phenomenon of brittle-to-ductile (BDT) transition is the main deformation characteristic during crack propagation in metallic materials [1-7]. The molecular dynamics (MD) simulations, which can provide the microstructure evolution of the materials, is a valuable tool and used to simulate the behaviour of crack propagation. The study results show that the phase transition and recrystallization are found at crack tip in body-centered cubic (bcc) iron at a higher loading level for $\{110\}\langle 110\rangle$ and $\{111\}\langle 110\rangle$ cracks [8-9]. Uhnakova et al [10-11] also predicted the emitting of dislocations at crack tip and analyzed the shielding or anti-shielding effects of dislocations and twins using MD simulations in bcc iron. In addition, the interaction between crack tip and pre-existing dislocations was also investigated, and indicated that it could cause the generation and motion of new dislocations at crack tip [12]. Meanwhile, much attention had been devoted to the investigation of crack propagation behaviour under cyclic loading [13-15].

In the studies of fatigue crack propagation behaviour, many researchers have been achieved significant results. It is concluded that the persistent slip bands (PSBs), voids and twins are observed at crack tip in the process of fatigue crack propagation for face-center cubic (fcc) metals [16-17]. Nishimura and Miyazaki [18] also investigated the interaction between the crack and two tilt grain boundaries using MD simulations and indicated that the phase transition and vacancies caused by the emission and absorption of dislocations were observed around the crack tip. Tang et al [19] analyzed

the fatigue crack propagation behaviour in magnesium single crystal under cyclic loading and revealed that the fatigue crack growth rate and the crack path varied with the crystallographic orientation of initial crack, and the strain rate and temperature had an important influence on crack growth rate. Uhnakova et al [20] investigated the ductile-brittle behaviour of an edge $(\bar{1}10)$ [110] crack in bcc iron at room temperature using MD simulations, the results revealed that the crack emitted dislocations in the inclined $\langle 111 \rangle \{112\}$ slip system under cyclic loading. Prahl et al [21] analyzed the behaviour of ductile-brittle at the (110)[001] crack in bcc iron crystal loaded monotonically in mode I, the fracture experiment showed that the cracks were deviated along $\{100\}$ planes and the fracture was accompanied by dislocation slip and twinning, and also indicated that 3D simulations using molecular dynamics simulations contributed to the understanding of crack propagation. Anna et al [22] presented 3D molecular simulations of edge crack (001) [110] in bcc iron under stress cyclic loading in mode I and II at room temperature, and showed that the crack (001) [110] loaded cyclically in mode I generated dislocations in oblique slip systems $\langle 11\bar{1} \rangle \{011\}$, further oblique twins in $\langle 111 \rangle \{11\bar{2}\}$ and inclined twins in slip systems $\langle 1\bar{1}1 \rangle \{\bar{1}12\}$ at higher loading.

This paper was devoted to investigating the edge crack propagation behaviour in bcc iron single crystal under cyclic loading using MD simulations. The models of (010)[001] crack, $(\bar{1}10)$ [110] crack and (111)[$11\bar{2}$] crack were used to study the behaviour of fatigue crack propagation. The deformation characteristics of crack tip were displayed. The effects of temperature on fatigue crack propagation were discussed for all the crack models, and the crack growth rate and stress intensity factor threshold were given under various temperatures.

2. Atomistic model and simulation method

The specimens of initial crack models were sketched in Figure 1(a). Pre-existing edge crack was built by removing atoms in iron single crystal. The crack surface was perpendicular in the y- direction and the crack front was oriented along the z- direction. The (010) [001] crack, $(\bar{1}10)$ [110] crack and (111)[$11\bar{2}$] crack were created, and the loading directions were [010], $[\bar{1}10]$ and [111], respectively. For the crack models, the numbers in parentheses represented initial crack plane and those in square brackets represented the front of initial crack. The periodic boundary was applied in z- direction and other directions were applied to non-periodic boundary. About five atomic layers lied in upper and lower boundaries were fixed and the cyclic loading was applied in y-direction. All the crack models were built with approximate dimensions of $57.2\text{nm} \times 57.2\text{nm} \times 5.72\text{nm}$ in x-, y- and z- direction, the total number of atoms was 1600000. The initial crack length was 5.72 nm, as 10 percent of the length of simulation boxes. Figure 1(b) showed the mode of strain cyclic loading, the initial strain amplitude of cyclic loading was 0.01 and the strain ratio was at the level of $R = \varepsilon_{\min} / \varepsilon_{\max} = 0.5$. Before cyclic loading, all the crack models were relaxation at various simulated conditions and reached equilibrium. The numbers of cyclic loading ranged from 1 to 15 for all crack models.

In the MD simulations, the interactions between atoms were described by a modified analytic embedded atom method (MAEAM), which had been applied successfully for the studies of metallic microstructure and melting simulations [23-27]. The MAEAM is a type of EAM potential and its formalisms is

$$E_i = \frac{1}{2} \sum_{j \neq i} \phi(r_{ij}) + F(\rho_i) + M(P_i) \quad (1)$$

where $\phi(r_{ij})$ is the pairwise interaction, $F(\rho_i)$ present the embedding energy, $M(P_i)$ is an extra energy-modified term that represents the contribution of non-spherical symmetry coming from each neighbor atom j with respect to the spherically symmetric atomic electron density.

The microstructure evolution was analyzed with common neighbor analysis (CNA) proposed by Honeycutt and Andersen [28], which provided the details of evolution process of fatigue crack propagation. The MD code of LAMMPS was used to study the fatigue crack propagation in this paper [29].

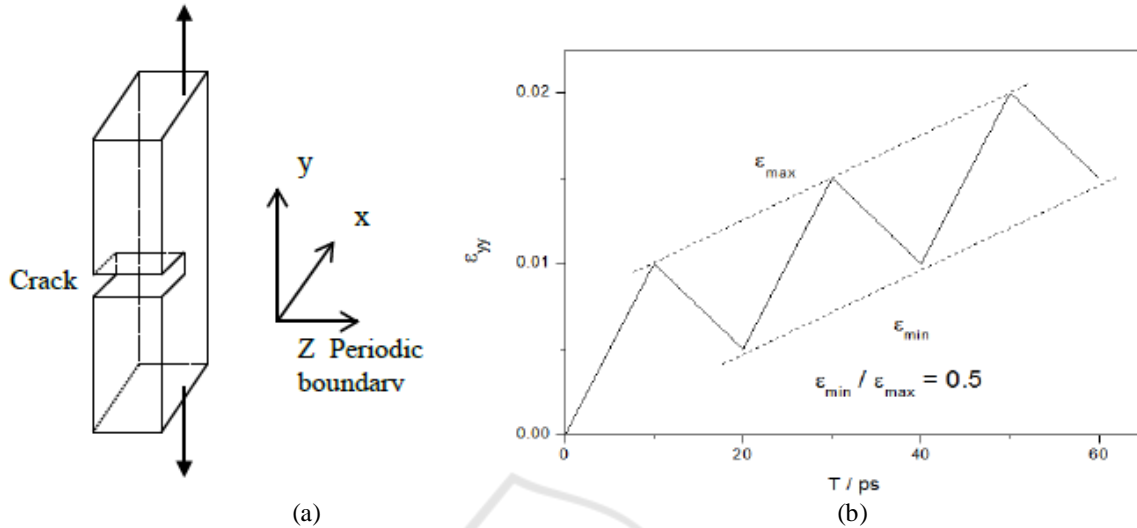


Figure 1. (a) Geometry of the atomistic model, (b) the mode of cyclic loading.

3. Results and discussion

3.1. Fatigue crack growth in iron single crystal

In this section, we investigated the behaviour of fatigue crack propagation in iron single crystal at room temperature. The stress intensity factor (K_I), which described the blunting phenomenon at crack tip, was calculated by Griffith level $K_I = K_G = F_l \sigma_A (\pi l_0)^{1/2}$, σ_A was the applied stress, l_0 was the crack length, $F_l = 1.16$ was the boundary correction factor [4, 20]. For fatigue crack propagation, the stress intensity factor range (ΔK) was calculated by $\Delta K = K_{\max} - K_{\min}$, the values of the maximum (σ_{\max}) and minimum (σ_{\min}) stresses were used to calculate K_{\max} and K_{\min} , The ΔK was between the threshold of stress intensity factor range (ΔK_{th}) and the crack fracture toughness (K_{Ic}). As the value of ΔK were larger than ΔK_{th} , the crack began to cleavage. Figure 2 showed fatigue crack propagation behaviour analyzed by CNA for (010)[001] crack in iron single crystal at room temperature. In Figure 2, the blue color denoted the perfect iron lattice (with coordination number KNT=14), the green color represented the slip bands (KNT=16). Observed from the (001) plane of model, up to cycle 5, the shearing slip bands were observed around the crack tip and the slip systems were along $\langle 111 \rangle \{110\}$ slip systems as the result of local stress concentration at crack tip. The Schmid factor described the slip systems was given and the value was 0.41, which was consistent with the inclined systems $\{110\}$ simulated by Alena [20]. As the cyclic loading increased, the plastic deformation zones were expansion, and blunting atom occurred at crack tip due to stress concentration at cycle 6, and we obtained $K_G = 2.043 \text{ MPa m}^{1/2}$ and $\Delta K_{th} = 0.299 \text{ MPa m}^{1/2}$ at the moment. In the case of cycle 7, the crack presented ductile fracture and propagated in the form of sharp crack along with $[11\bar{1}]$ direction, and the slip bands appeared at sharp crack tip. Figure 3(a) and Figure 3(b) showed the detail and 3D visualization of slip bands at crack tip at cycle 7. From Figure 3, it was clear that the complete dislocation obtained from crack tip due to influence of the periodic boundary conditions.

The shearing slip bands caused by the motion of dislocations significantly decreased the crack growth rate by reducing stress concentration at crack tip. At cycle 8, the crack propagated continually in accompany with the slip bands of crack tip expanding, the blunting and voids were the main deformation mechanisms of crack tip caused by the stress concentration and induced the fatigue crack propagation.

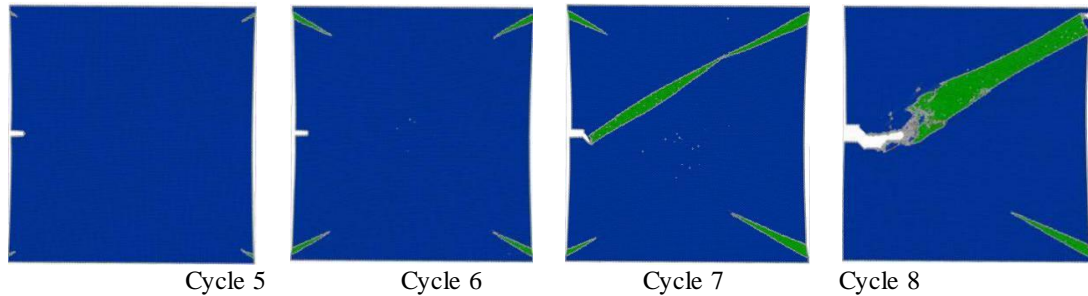


Figure 2. The microstructure evolution of crack tip analyzed by CNA for (010)[001] crack under cyclic loading in iron single crystal.

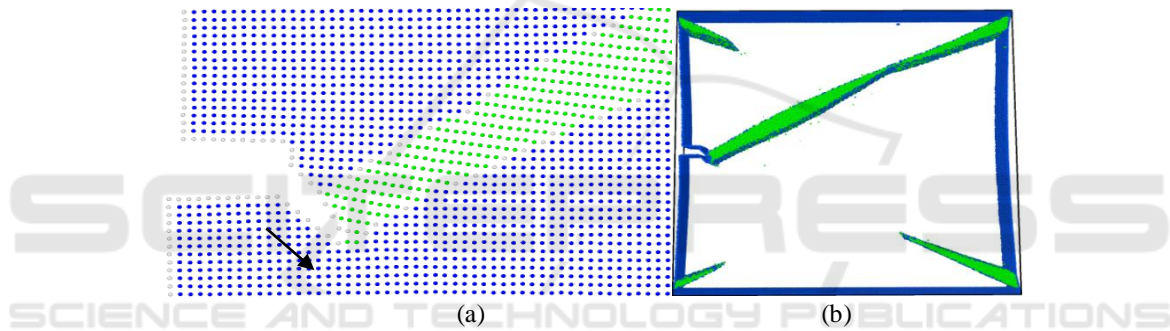


Figure 3. (a) The generation of slip band (green atoms in front of the crack) at crack tip in surface layer of (001) of (010)[001] crack at cycle 7, (b) 3D visualization of slip bands around the crack tip.

Figure 4 showed the deformation characteristics of crack tip at different crack models as the fatigue crack propagated. The blue color represented the iron atoms and the green color represented the slip bands. For $(\bar{1}10)[110]$ crack and $(111)[11\bar{2}]$ crack, we obtained $K_G = 2.054 \text{ MPa m}^{1/2}$, $\Delta K_{th} = 0.216 \text{ MPa m}^{1/2}$ and $K_G = 2.143 \text{ MPa m}^{1/2}$, $\Delta K_{th} = 0.116 \text{ MPa m}^{1/2}$, respectively. These values were lower comparing with (010)[001] crack. Figure 4(a) showed the microstructure evolution of crack tip analyzed by CNA for $(\bar{1}10)[110]$ crack under strain cyclic loading in iron single crystal. The results indicated that the main deformation mechanisms were shearing slip bands at crack tip, and the slip system were $(011)[\bar{1}\bar{1}1]$. The crack presented brittle rupture and the path of crack propagation was along $[\bar{1}10]$ direction. Figure 5(a1) and Figure 5(a2) presented the generation of slip bands at crack tip in surface layer (110) of $(\bar{1}10)[110]$ crack at cycle 6. In comparison with the stress cyclic loading in the $(\bar{1}10)[110]$ crack, the oblique slip changed and the $\{112\}\langle 111 \rangle$ slip systems $[20]$ were not observed. Figure 4(b) presented the behaviour of fatigue crack propagation for $(111)[11\bar{2}]$ crack. The results showed that the formation of micro-crack at crack tip induced the crack propagation along $[\bar{1}10]$ direction in accompany with blunting phenomenon caused by stress concentration, and the dislocations were the dominant deformation around the crack tip. Figure 5(b1) and Figure 5(b2)

showed the deformation mechanisms of crack tip in surface layer $(11\bar{2})$ of $(111)[11\bar{2}]$ crack at cycle 4. The vacancies were also observed at crack tip. As seen from above results, it was shown that the front of initial crack had an important influence on the deformation mechanisms of crack tip for iron single crystal under cyclic loading at room temperature.

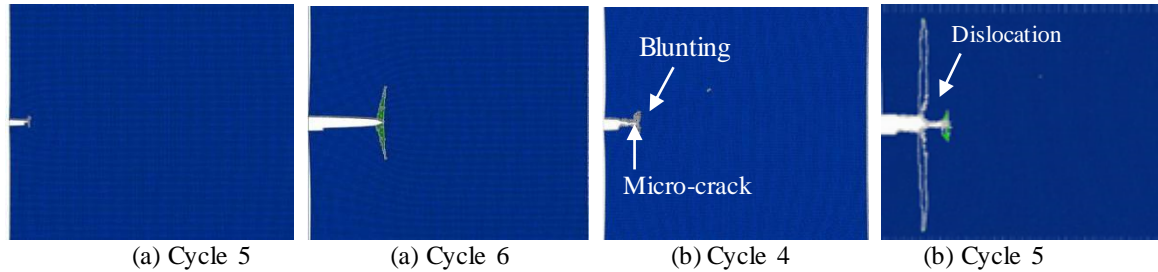


Figure 4. The microstructure evolution of crack tip analyzed by CNA for (a) $(\bar{1}10)[110]$ crack and (b) $(111)[11\bar{2}]$ crack under cyclic loading in iron single crystal.

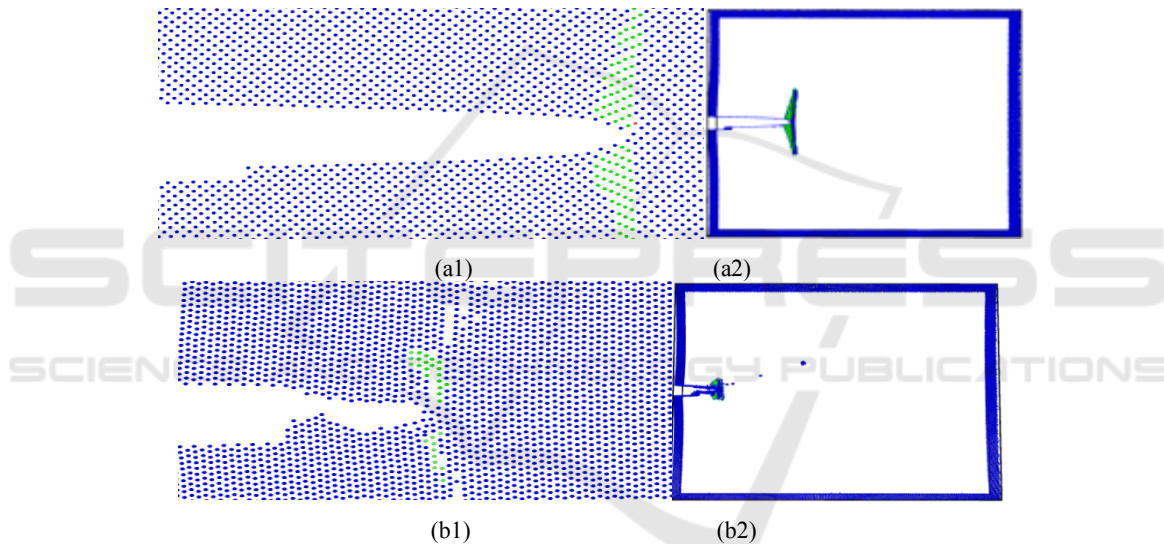


Figure 5. (a1) The generation of slip bands at crack tip in surface layer (110) of $(\bar{1}10)[110]$ crack at cycle 6, (a2) 3D visualization of dislocations emission around the crack tip in $(\bar{1}10)[110]$ crack (green atoms in front of the crack), (b1) The deformation mechanisms of crack tip in surface layer $(11\bar{2})$ of $(111)[11\bar{2}]$ crack at cycle 4, (b2) 3D visualization of deformation mechanism around the crack tip in $(111)[11\bar{2}]$ crack (green atoms in front of the crack).

3.2. Crack growth rate

In this section, the variation of crack length with number of cycles for various crack models was calculated by tracking the position of crack tip as shown in Figure 6. The simulation results showed that the length of $(\bar{1}10)[110]$ crack grew faster comparing with other crack models. The average crack growth rates of $(010)[001]$ crack, $(\bar{1}10)[110]$ crack and $(111)[11\bar{2}]$ crack by fitting the variation of crack length were 2.46×10^{-9} m/cycle, 6.59×10^{-9} m/cycle and 2.19×10^{-9} m/cycle, respectively. So the crack growth rate of $(\bar{1}10)[110]$ crack was maximum, and the crack growth rate of $(111)[11\bar{2}]$ crack was minimum. The reasons resulting in the differences of crack growth rate for

the cracks of various orientations were the differences of deformation mechanisms of crack tip. Besides, the interaction between the crack growth rate (da/dN) and the stress intensity factor range (ΔK) was calculated from the known relations $da/dN = (da/dN)_{th} (\Delta K / \Delta K_{th})^n$, where a is the crack half length, N is the number of cycles, “th” was the threshold, “n” was Paris exponent. The value of Paris exponent was obtained by the results of atomistic simulation of fatigue behaviour in bcc iron [10]. Figure 7 presented the crack growth rate with the change of stress intensity factor range in different crack models. The results showed that the values of da/dN ranged from 10^{-11} to 10^{-9} m/cycle. The ΔK of the crack models ranged from 0.105 to $0.548 \text{ MPa}\sqrt{\text{m}}$, these values were lower comparing with the center crack propagation in iron single crystal [30]. At the same time, the crack growth rate of all the crack models increased as the increase of ΔK , and the $(\bar{1}10)[110]$ crack had the maximum rate of crack propagation comparing with other crack models.

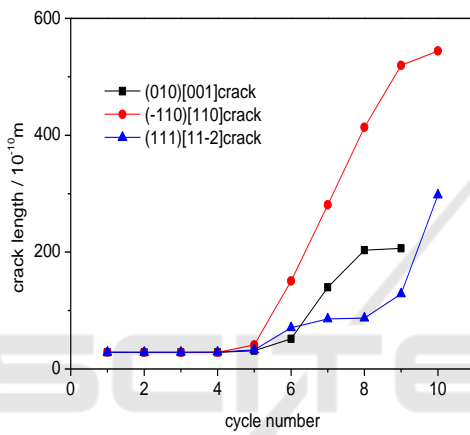


Figure 6. The variation of crack length was stress calculated at crack the model of different front under cyclic loading.

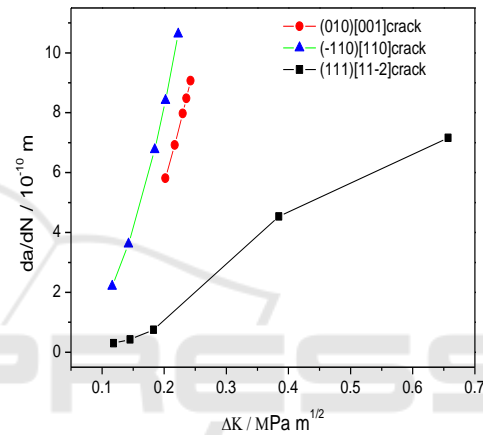


Figure 7. Crack growth rate ranged with the intensity factor range for (010)[001] crack, $(\bar{1}10)[110]$ crack and (111)[11 $\bar{2}$] crack.

3.3. Temperature effect

In order to analyze the temperature effects on the behaviour of fatigue crack propagation, various temperatures including 300K, 400K, 500K, and 600K were applied to all the crack models. The blue, green and red colors represented bcc structure, fcc slip and hcp structure in Figure 8, Figure 9 and Figure 10, respectively. Figure 8 presented the behaviour of fatigue crack propagation for (010)[001] crack at various temperatures. It showed that the dominant deformation mechanisms were shearing slip bands, blunting and linkage of voids at the tip of crack as the increasing temperature. The crack presented ductile fracture as crack propagation at temperature of 300K. From 400K to 600K, the crack appeared softening and the growth path of crack changed with the formation of sharp crack at crack tip. Besides, the phase transition of local region was also observed in the front of crack from 400K to 600K. Figure 9 showed the propagation behaviour of crack for $(\bar{1}10)[110]$ crack at various temperatures in single crystal iron. The results indicated that the deformation mechanism of crack tip had changed at higher temperatures, and the voids were the dominate mechanism at crack tip at 400K. From 500K to 600K, some microcracks appeared at the crack front and induced the structure failure. For the (111)[11 $\bar{2}$] crack, temperature mainly affected the crack propagation path as shown in Figure 10. At room temperature the (111)[11 $\bar{2}$] crack advanced along [110] direction, nevertheless, the path of crack propagation deviated from the [110] direction as the temperature rose. At high temperatures,

the sharp crack that formed along [111] direction at crack tip had grown larger and forced the path of crack propagation to widen that resulting in the rate of crack propagate increasing for $(111)[11\bar{2}]$ crack.

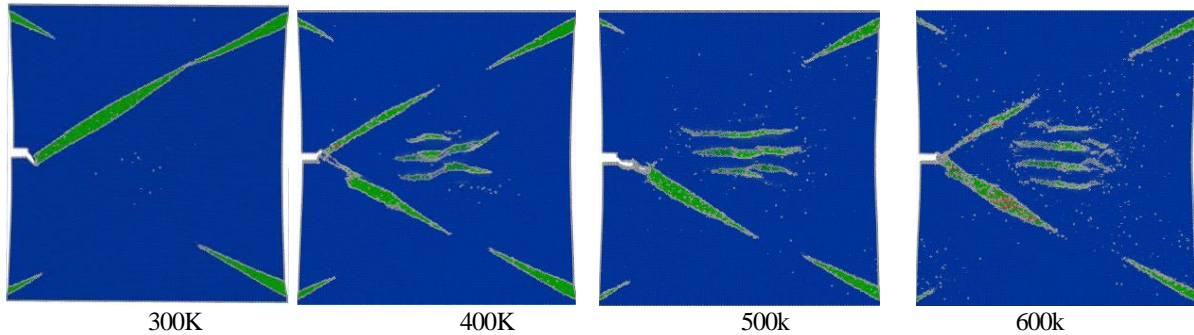


Figure 8. The deformation behaviour of crack tip analyzed by CNA for $(010)[001]$ crack at various temperatures in iron single crystal.

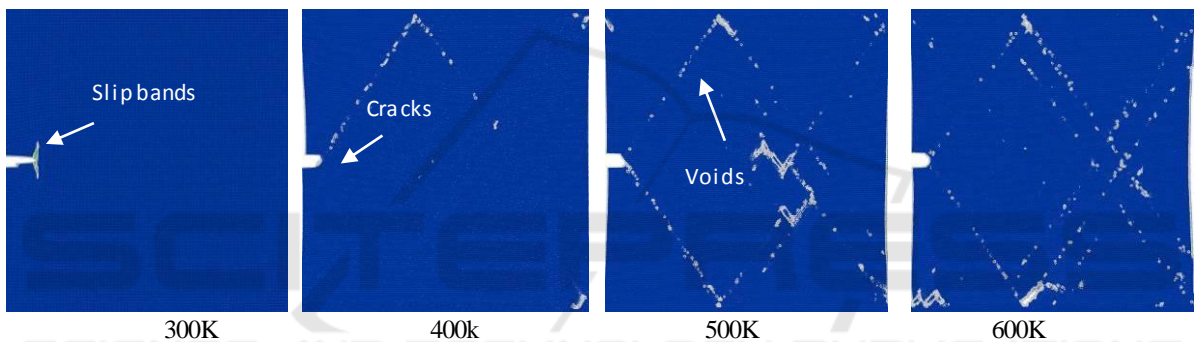


Figure 9. The deformation behaviour of crack tip analyzed by CNA for $(\bar{1}10)[110]$ crack at various temperatures in iron single crystal.

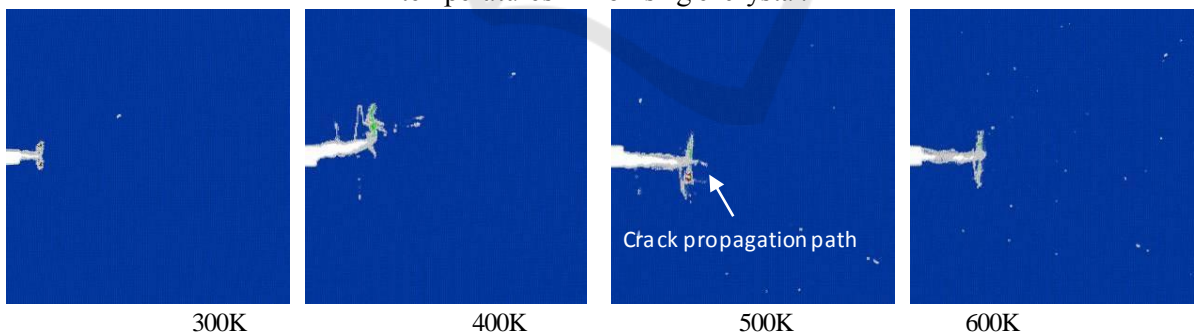


Figure 10. The deformation behaviour of crack tip analyzed by CNA for $(111)[11\bar{2}]$ crack at various temperatures in iron single crystal.

Figure 11 showed the variation of crack length for $(010)[001]$ crack, $(\bar{1}10)[110]$ crack and $(111)[11\bar{2}]$ crack at various temperatures with number of cycles in iron single crystal. In $(010)[001]$ crack, the results indicated that the crack growth rate was basically to assume decline with the increasing temperature in addition to 500K. For the special temperature of 500K, the crack growth rate increased comparing with others. The reason was that the formation of voids around the crack tip led to the increasing of crack propagation rate. In $(\bar{1}10)[110]$ crack, the obtained from the variation of crack length with the number of cycles at various temperatures showed that the fatigue crack

growth rate decreased as the temperature rose, because the materials became softening with the increasing temperature and effectively inhibited the fatigue crack propagation. However, the (111)[11 $\bar{2}$] crack presented a different temperature effect, the fatigue crack growth rate increased with the increasing temperature as showed in Figure 11(c).

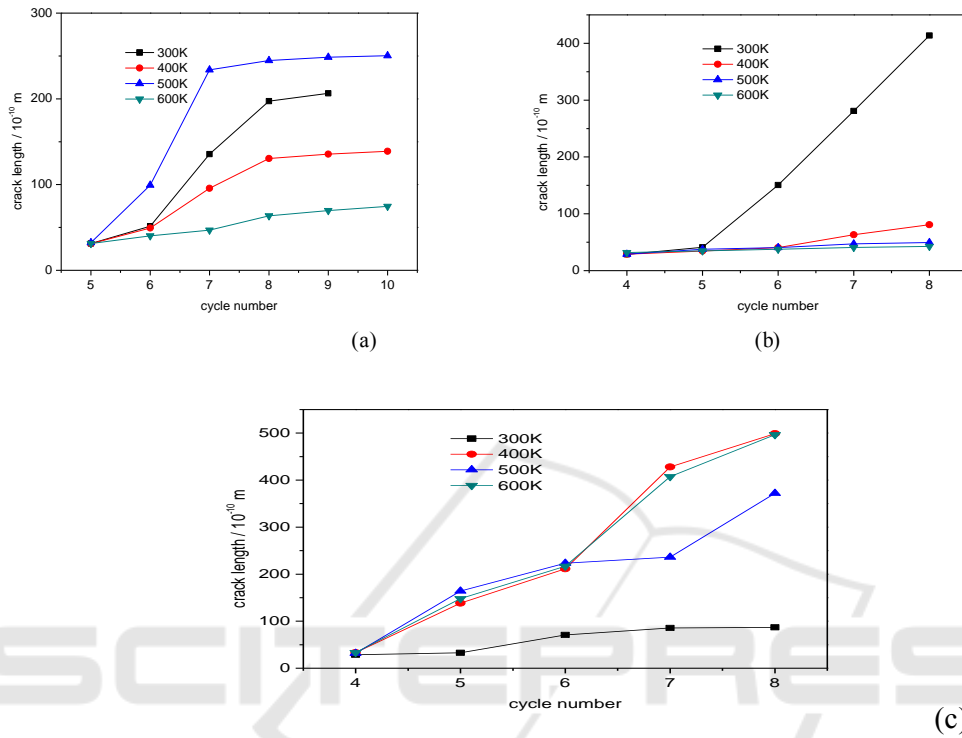


Figure 11. The variation of crack length for (a): (010) [001] crack, (b): (1-10) [110] crack and (c): (111) [11 $\bar{2}$] crack at various temperatures under cyclic loading in iron single crystal.

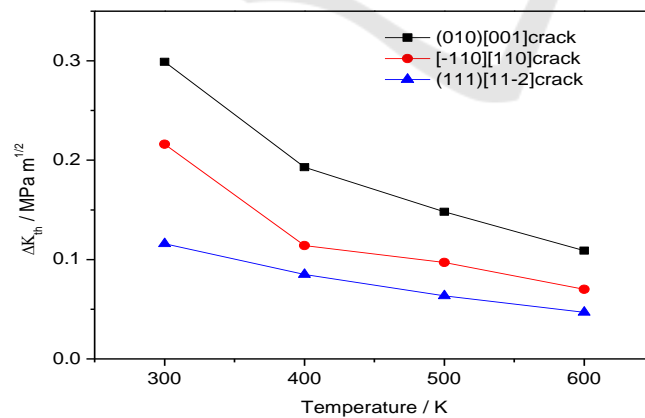


Figure 12. The variation of the stress intensity factor threshold (ΔK_{th}) for (010) [001] crack, (1-10) [110] crack and (111)[11 $\bar{2}$] crack at various temperatures in iron single crystal.

The fracture toughness of crack tip under cyclic loading is described by the given value of the stress intensity factor threshold (ΔK_{th}) which was based on the Griffith fracture theory. As the stress

intensity factor ΔK was below the value of ΔK_{th} , the mechanical load can not lead to the crack initiation and propagation. Figure 12 showed the variation of the threshold value of stress intensity factor ΔK_{th} at various temperatures for (010) [001] crack, $(\bar{1}10)[110]$ crack and $(111)[11\bar{2}]$ crack. The simulation results presented that the ΔK_{th} decreased with the increasing temperature for all the crack models, which was caused by the various deformation mechanisms of crack tip. In (010)[001] crack, as the temperature rose, the slip bands of crack tip increased as shown in Figure 8 so that the stress concentration of crack tip was relaxed, and led to the ΔK_{th} decreasing. For $(\bar{1}10)[110]$ crack and $(111)[11\bar{2}]$ crack, a large number of voids and the formation of sharp crack destroyed the stress concentration of crack tip at higher temperatures as shown in Figure 9 and Figure 10 so that the driving force of crack tip decreased, thus resulting in the decreasing of ΔK_{th} . So the fracture mode of material was the ductile fracture caused by crack propagation with the increasing temperatures, and the high temperature was effective on the resistance of fatigue crack propagation.

4. Conclusions

The behaviour of fatigue crack propagation with pre-existing edge crack was investigated in iron single crystal under strain cyclic loading using MD simulations. The deformation mechanisms of crack tip were depended on the crack front. In (010)[001] crack, the crack presented ductile fracture and the dominant mechanism were slip bands and the slip systems was $\langle 111 \rangle \{110\}$. For $(\bar{1}10)[110]$ crack, the crack propagation was brittle rupture and the slip bands was along (011) $[\bar{1}\bar{1}1]$ system. However, in $(111)[11\bar{2}]$ crack, the micro-crack occurred at crack tip and induced the crack propagation, and the main deformation mechanisms of crack tip were vacancies and dislocations. Meanwhile, the $(\bar{1}10)[110]$ crack had the maximum crack growth rate comparing with (010)[001] crack and $(111)[11\bar{2}]$ crack.

The effects of temperature on fatigue crack propagation in iron single crystal were studied. For (010)[001] crack, at high temperature the deformation mechanisms of crack tip were the linkage of voids slip bands and phase transition that happened in front of crack tip. The crack growth rate decreased with increasing temperature except for 500K which was caused by the formation of the linkage of voids at crack tip. For $(\bar{1}10)[110]$ crack, as the temperature rose, voids were the predominate deformation around the crack tip, new micro-cracks was formation at the crack front, and the fatigue crack growth rate decreased. However, the fatigue crack growth rate of $(111)[11\bar{2}]$ crack increased with the increasing temperature. Besides, the threshold of stress intensity factor of all the crack models decreased with the increasing temperature.

Acknowledgements

This work is supported by the “16BSQD05 and the Key Youth Foundation of Hunan Provincial Education Department (No.17B180) and the Jiangxi Provincial Natural Science Foundation of China (No. 20171BAB216001) and Scientific Research Project of Jiangxi Provincial Education Department (No. GJJ161242).

References

- [1] Gumbsch P, Riedle J, Hartmaier A and Fischmeister H F 1998 Controlling factors for the brittle-to-ductile transition in tungsten single crystals *Science* 282 1293-5
- [2] Hartmaier A and Gumbsch P 2005 Thermal activation of crack-tip plasticity: The brittle or ductile response of a stationary crack loaded to failure *Phys Rev B* 71 024108
- [3] Smida T and Bosansky J, Micromechanism of cleavage fracture in ferritic steels *Kovove Mater* 40(2002) 146

- [4] Spielmannova A, Machova A and Hora P 2007 Crack orientation versus ductile-brittle behaviour in 3D atomistic simulations *Mater Sci Forum* 567-568 61
- [5] Khantha M, Pope D P and Vitek V 1994 Dislocation screening and the brittle-to-ductile transition: a Kosterlitz-Thouless type instability *Phys. Rev. Lett* 73 684-7
- [6] Ohr S M 1985 An electron microscope study of crack tip deformation and its impact on the dislocation theory of fracture *Mater. Sci. Eng.* 72 1
- [7] Vehoff H and Neumann P 1979 In situ SEM experiments concerning the mechanism of ductile crack growth *Acta Metall* 27 915
- [8] Guo Y F, Wang Y S and Zhao D L 2007 Atomistic simulation of stress-induced phase transformation and recrystallization at the crack tip in bcc iron *Acta Metall* 55 401-407
- [9] Guo Y F and Zhao D L 2007 Atomistic simulation of structure evolution at a crack tip in bcc-iron *Materi Sci Eng A* 448 281-186
- [10] Uhnakova A, Machova A and Hora P 2009 Crack-induced stress, dislocations and acoustic emission by 3-D atomistic simulation in bcc iron *Acta Metall* 57 4065-4073
- [11] Uhnakova A, Machova A and Hora P 2010 Transonic twins in 3D bcc iron crystal *Comput. Mater. Sci* 48 296-302.
- [12] Bitze K E and Gumbsch P 2013 Mechanisms of dislocation multiplication at crack tips *Acta Metall* 61 1394-1403
- [13] Deshpande V S, Needleman A and Van der Giessen E 2002 Discrete dislocation modeling of fatigue crack propagation *Acta Mater* 50 51
- [14] Potirniche G P, Horstemeyer M F, Jelinek B and et al 2005 Fatigue damage in nickel and copper single crystals at nanoscale *Int. J. Fatigue* 27 1179-1185
- [15] Potirniche G P, Horstemeyer M F, Gullett P M and et al 2006 *Proceedings Roral Society A* 462 3707-3731
- [16] Farkas D, Willemann M, Hyde B 2005 Atomistic mechanisms of fatigue in nanocrystalline metals *Phys. Rev. Lett* 94 165502
- [17] Potirniche G P and Horstemeyer M F 2006 On the growth of nanoscale fatigue cracks *Philos. Mag. Lett* 86 (3) 185-193
- [18] Nishimura K and Miyazaki N 2004 Molecular dynamics simulation of crack growth under cyclic loading *Comput. Mater. Sci* 31 269-278
- [19] T Tang, S Kim and M F Horstemeyer 2010 Fatigue crack growth in magnesium single crystals under cyclic loading: Molecular dynamics simulation *Comput. Mater. Sci* 48 42439
- [20] Uhnakova A, Machova A and Hora P 2011 3D atomistic simulation of fatigue behaviour of a ductile crack in bcc iron *Int. J. Fatigue* 33 1182-1188
- [21] Prahl J, Machov áA, Spielmannov áA and et al 2010 *Engineering Fracture Mechanics* 77 184-192
- [22] Machova A, Pokluda J, Uhnakova A and Hora P, 2014 3D atomistic studies of fatigue behaviour of edge crack (001) in bcc iron loaded in mode I and II *Int. J. Fatigue* 66 11-19
- [23] Luo W H, Hu W Y, and Xiao S F 2008 Size Effect on the Thermodynamic Properties of Silver Nanoparticles *J. Phys. Chem. C* 112 2359-2369
- [24] Luo W H, Hu W Y, and Xiao S F 2008 Melting temperature of Pb nanostructural materials from free energy calculation *J. Chem. Phys.* 128 074710
- [25] Xiao S F, Hu W Y, and Yang J Y, 2006 Melting temperature: From nanocrystalline to amorphous phase *J. Chem. Phys* 125 184504
- [26] Xiao S F and Hu W Y 2006 Comparative study of microstructural evolution during melting and crystallization *J. Chem. Phys.* 125 014503
- [27] Wang K, Xiao S F, Deng H Q, Zhu W J, Hu W Y 2014 An atomic study on the shock-induced plasticity and phase transition for iron-based single crystals *Int. J. Plasticity* 59 180-198
- [28] J Dana Honeycutt and Hans C, Andersen 1987 Molecular Dynamics Study of Melting and Freezing of Small Lennard-Jones Clusters *J. Phys. Chem* 91 4950-4963
- [29] Plimpton S 1995 Fast Parallel Algorithms for Short-Range Molecular Dynamics *J Comp Phys* 117 (1) 1-19
- [30] Ma L, Xiao S F, Deng H Q and Hu W Y 2014 Molecular dynamics simulation of fatigue crack

propagation in bcc iron under cyclic loading *Int. J. Fatigue* 68 253

